Science of the Total Environment 793 (2021) 148578

Contents lists available at ScienceDirect

Science of the Total Environment

journal homepage: www.elsevier.com/locate/scitotenv

Using spectral indices as early warning signals of forest dieback: The case of drought-prone *Pinus pinaster* forests

Daniel Moreno-Fernández [a,*], Alba Viana-Soto [b], Julio Jesús Camarero [c], Miguel A. Zavala [a], Julián Tijerín [a], Mariano García [b]

[a] Universidad de Alcalá, Departamento de Ciencias de la Vida, Forest Ecology and Restoration Group, Edificio Ciencias, Campus Universitario, 28871 Alcalá de Henares, Madrid, Spain
[b] Universidad de Alcalá, Departamento de Geología, Geografía y Medio Ambiente, Environmental Remote Sensing Research Group. Calle Colegios 2, 28801 Alcalá de Henares, Spain
[c] Instituto Pirenaico de Ecología (IPE-CSIC), Avda. Montañana 1005, E-50192 Zaragoza, Spain

HIGHLIGHTS

- Trend of wetness indices as a potential early warning signal of forest dieback
- Water content and greenness of healthier plots was larger since the drought of 1993–95.
- Land surface phenology metrics showed no significant differences among damage levels.
- Dieback was linked to the concurrence of previous droughts and a recent intense drought.

GRAPHICAL ABSTRACT

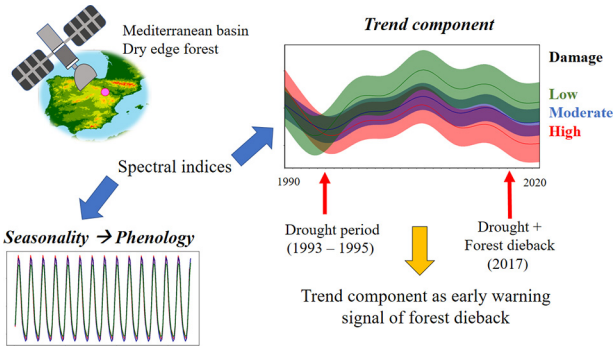

ARTICLE INFO

Article history:
Received 9 April 2021
Received in revised form 14 June 2021
Accepted 16 June 2021
Available online 19 June 2021

Editor: Manuel Esteban Lucas-Borja

Keywords:
Forest die-off
Tree mortality
BEAST
Phenometrics
Drought
Decay

ABSTRACT

Forest dieback processes linked to drought are expected to increase due to climate warming. Remotely sensed data offer several advantages over common field monitoring methods such as the ability to observe large areas on a systematic basis and monitoring their changes, making them increasingly used to assess changes in forest health. Here we aim to use a combined approximation of fieldwork and remote sensing to explore possible links between forest dieback and land surface phenological and trend variables derived from long Landsat time series. Forest dieback was evaluated in the field over 31 plots in a Mediterranean, xeric *Pinus pinaster* forest. Landsat 31-year time series of three greenness (EVI, NDVI, SAVI) and two wetness spectral indices (NMDI and TCW) were derived covering the period 1990–2020. Spectral indices from time series were decomposed into trend and seasonality using a Bayesian estimator while the relationships of the phenological and trend variables among levels of damage were assessed using linear and additive mixed models. We have not found any statistical pieces of evidence of extension or shortening patterns for the length of the phenological season over the examined 31-year period. Our results indicate that the dieback process was mainly related to the trend component of the spectral indices series whereas the phenological metrics were not related to forest dieback. We also found that plots with more dying or damaged trees displayed lower spectral indices trends after a severe drought event in the middle of the 1990s, which confirms the Landsat-derived spectral indices as indicators of early-warning signals. Drops in trends occurred earlier for wetness indices rather than for greenness indices which suggests that the former could be more appropriate for dieback detection, i.e. they could be used as early warning signals of impending loss of tree vigor.

* Corresponding author.
E-mail address: danielmorenofdez@gmail.com (D. Moreno-Fernández).

https://doi.org/10.1016/j.scitotenv.2021.148578

1. Introduction

Climate change and land-use changes are two of the main processes driving the global change in forest ecosystems (Hansen et al., 2001a, 2001b). Climate change involves an increment of the global air temperature but also more frequent climate extremes such as droughts, while land-use changes in forests are related to transformations from forested to non-forests lands (shrublands, crops, grasslands, etc.) and vice versa, or modifications of forest structure and species composition (Bonfils et al., 2020; Trumbore et al., 2015).

One of the main consequences of global change on forest ecosystems is the increment of dieback processes associated with extreme droughts and the alteration or intensification of pests and pathogens impacts on forests (Allen et al., 2015, 2010; Chen et al., 2018; Seidl et al., 2017; Simler-Williamson et al., 2019). Hence, many investigations have pointed out the forest dieback process characterized by canopy defoliation and growth decline resulting from drought events at different biomes (Allen et al., 2015; Camarero et al., 2015a, 2015b; Móricz et al., 2018; Xulu et al., 2018). When the species cannot adapt and respond to the new conditions, dieback processes may result in local extinction phenomena and species shifts (Aitken et al., 2008; Anderegg et al., 2013) with consequent loss of ecosystem services provision (Zhang et al., 2013).

One of the first visual symptoms of canopy dieback in affected trees is crown defoliation and brownness due to shoot and leaf death (Manion, 1981). Forest dieback and mortality can also be monitored or even forecasted through tree ring width inspection of dendrochronological records and analyses of early-warning growth signals (Camarero et al., 2015a, 2015b; Gazol et al., 2020). This technique, however, is usually limited to the tree or small spatial scales and has been shown not to apply to all species and situations (Cailleret et al., 2017). On the contrary, national forest inventories and monitoring plot networks have been used to assess forest health status at the continental and landscape scales via tree defoliation assessment (e.g., International Co-operative Programme on Assessment and Monitoring of Air Pollution Effects on Forests, hereafter ICP forests) but they can miss local information on dieback or mortality hotspots situated in extremely dry sites (de la Cruz et al., 2014; Moreno-Fernández et al., 2019). One of the drawbacks of these inventory data is that the interval between resampling cycles may preclude the detection of dieback hotspots triggered by recent droughts. Likewise, their limited spatial sampling, 10 km regular grid in the case of the ICP forest, may not be able to capture the dieback process until they are extensive. Remote sensing offers a sound alternative to field methods for monitoring forest dieback and tree vigor at large spatial scales by assessing the contribution of climatic variations and biological agents to changes in forest health based on the spectral changes associated to decline symptoms (Anderegg et al., 2019, 2015; Bell et al., 2018; Byer and Jin, 2017; Campbell et al., 2020).

Remote sensing techniques enable regional-to-continental assessments of forest health through temporal series of spectral indices (SIs) that combine alternative satellite bands related to the spectral characteristics of vegetation (Jiao et al., 2020; Marusig et al., 2020). Some of the most common SIs used in ecosystem monitoring are vegetation indices which are based on the estimation of absorbed photosynthetically active radiation. Another broad group of SIs includes wetness indices, which are focused on estimating the vegetation water content (Marusig et al., 2020).

Temporal changes in SIs are linked to ecosystem phenology, intra- and inter-annual climate variations, perturbations or changes in long-term environmental trends or successional dynamics, among other drivers (Hamunyela et al., 2016). Temporal SIs series can be decomposed into abrupt, gradual and seasonal changes. Disturbances affecting forest ecosystems, such as clear-fellings or windthrows or wildfires, are reflected as abrupt drops in the time series of SIs while gradual changes in temporal SIs series are driven by long-term environmental trends, chronic disturbances or successional dynamics (Verbesselt et al., 2010; Zhao et al., 2019b). From a temporal perspective, drought effects do not result in dramatic drops in the trend of a given index but are expected to cause subtle changes (Assal et al., 2016; Zhao et al., 2019b). Therefore, analysis of SI trends can be used for the identification of drought-prone vulnerable areas before dieback and massive mortality occur, i.e., early-warning detection (Anderegg et al., 2019; Rogers et al., 2018; Vicente-Serrano et al., 2016). Here, it is important to note that the response to water stress is functional-type dependent. Broadleaves can use the water stored in the heartwood during prolonged dry periods while conifers keep their water reserves mainly by real-time absorption (Goldsmith, 2013; Querejeta et al., 2007). As a consequence of prolonged dry periods photosynthetic activity and greenness drop. Therefore, wetness indices could be more appropriate to detect forest decline in earlier stages, especially for conifer species (Liu et al., 2021).

The seasonal and cyclical phenological behavior depends on the functional group of tree species and environmental conditions (Aragones et al., 2019; Kobayashi et al., 2018; Ryu et al., 2014). Seasonality metrics derived from SIs time series reflect the land surface phenological cycles and intra- and inter- annual oscillations, i.e., vegetation activity, at the ecosystem level (Garonna et al., 2014; Stöckli and Vidale, 2004). Thus, satellite-based phenological variables, so-called land surface metrics, have many applications within forest research including the discrimination of species and typologies (Aragones et al., 2019; Chakraborty et al., 2018) or the study of the dynamic response of forest ecosystems to climate change. For instance, the duration of the phenological season is determined by environmental conditions such as snow cover or summer drought (Recuero et al., 2019; White et al., 2009). Hence, because some conifers species growing in temperate and Mediterranean latitudes photosynthesize during the winter (Aragones et al., 2019), a mild-wet winter period could promote carbohydrate synthesis and storage and enhance stem growth in the following spring (Lebourgeois et al., 2010). In contrast, a warm-dry winter may weaken the tree hydraulic–carbohydrate system and reduce tree growth the following year (Earles et al., 2018). Furthermore, dry and warm spring-summer conditions could lead to canopy dieback and tree mortality in Mediterranean forests (Camarero et al., 2015a, 2015b). Since photosynthesis drives primary production and contributes to carbon uptake and tree growth it seems necessary to understand the aboveground phenological responses to environmental conditions (Ma et al., 2015).

Forests growing alongside the Mediterranean basin are especially vulnerable to climate change mainly due to summer droughts which are forecasted to increase in severity, frequency and extent (Gao and Giorgi, 2008; Giorgi and Lionello, 2008; Turco et al., 2017). This situation can be aggravated in single-species forests (Lebourgeois et al., 2013; Pretzsch et al., 2020), which have been widely favored or maintained during the last century (Valbuena-Carabaña et al., 2010; Varo-Martínez and Navarro-Cerrillo, 2021). Despite some efforts that have been done attempting to identify biotic information on the status of declining forests, including biochemical (Varo-Martínez and Navarro-Cerrillo, 2021) and physiological traits (Marusig et al., 2020), the information on the influence of phenological variables (e.g., start of the season, length of the season or peak greenness) on forest dieback derived from remote sensing in drought-prone forests, however, is hitherto lacking. The identification of phenological variables characterizing the dieback process could contribute to the spatial delineation of damaged areas as well as increase the knowledge of the response of forest ecosystems to the upcoming climatic shifts including aridification (Garonna et al., 2014; van Leeuwen et al., 2010). As regard forest phenology, summer drought results in low soil moisture and high leaf vapor pressure constraining the photosynthesis activity and the leaf water content (Calama et al., 2013; Peñuelas et al., 2004). Furthermore, Camarero et al. (2016) stated that drought impairs xylem phenology in Mediterranean forests. Then, it could be expected that healthier stands, i.e., those more resilient to drought, depicted longer phenological seasons and started growing earlier than damaged stands as healthier trees can

better photosynthesize under adverse climatic conditions during the growing season.

In this work, we used phenological and trend metrics derived from time series of five SIs obtained from Landsat images coupled with forest data measured in the field to characterize a recent dieback process induced by drought in a *Pinus pinaster* Ait. (commonly known as Maritime pine) Mediterranean forest. The specific objectives of this work were: i) to analyze to what extent phenological and trend variables derived from Landsat series are affected by forest dieback, and ii) to investigate whether Landsat metrics (SIs) are capable to identify early warning signals of forest dieback. We expect that the most affected stands will display shorter phenological seasons, perhaps because they have less access to soil water than healthier stands. We also hypothesized that current health status is linked to a cumulative stress or carryover effect resulting from previous droughts and a recent intense drought acting as dieback trigger.

2. Material and methods

2.1. Study area and data gathering

The study area is located in a natural forest dominated by *P. pinaster* ("Sistema Ibérico Central" provenance), which represents some of the dry-continental edges of the natural distribution of the species. The forest is placed in inner north-eastern Spain (Miedes de Aragón, 41° 16′ 13″ N, 1° 26′ 9″ W) at an altitude of c.a. 1050 m a.s.l. on acid soils

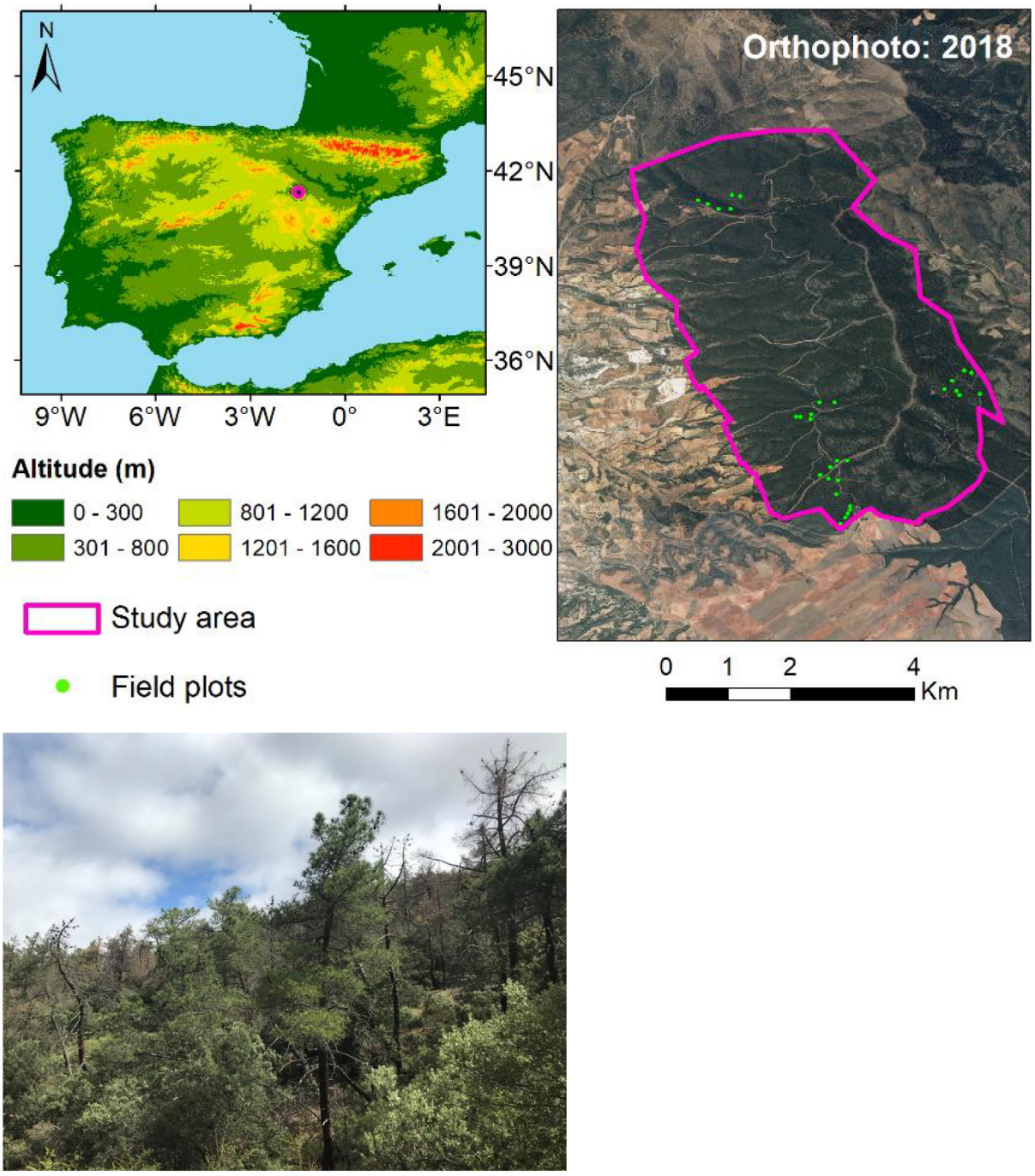

Fig. 1. Location of the study area and a view of a *Pinus pinaster* stand severely impacted by drought-induced dieback. Note the undamaged Holm oak (*Quercus ilex*) individual in the right, lower corner of the image.

(Fig. 1). In this area, the total annual rainfall is 404 mm, and the average annual temperature is 12.9 °C (calculated from the nine nearest climatic stations). Despite *P. pinaster* is the dominant species, *Quercus ilex* L. occurs in the midstory although it rarely exceeds a diameter at breast height (dbh, measured at 1.3 m) larger than 10 cm. Shrub species, such as *Cistus* spp., *Calluna vulgaris* (L.) Hull and *Arctostaphylos uva-ursi* (L.) Spreng., also grow in the understory. Both *P. pinaster* and the understory species are evergreen species.

Forest managers detected forest dieback in *P. pinaster* trees in 2017, but they did not identify any pathogen or insect defoliator driving this process so that it was assumed that it was related to the severe 2017 drought, which was the strongest over the last 60 years (Fig. 2A). The dieback was more intense in south-facing slopes, i.e., in those areas that receive more sunlight and are warmer and xeric. The dieback severity, however, is not uniform across the whole south-facing slopes but it occurs in patches with different degrees of crown damage and tree mortality. Previous studies have reported similar processes for this species in other areas in Central Spain subjected to similar climatic conditions but with different soil properties (Férriz et al., 2021; Prieto-Recio et al., 2015). Although there has been a lack of silvicultural operations over the last three decades, some fellings have been carried out from 2020 to remove dead trees and to reduce competition. We focused on non felled stands to avoid biases related to stand structure.

To achieve our goals, we installed 31 17-m-radius circular plots, equivalent to the area of a Landsat pixel, from October 2020 to February 2021 aiming at covering a wide range of degrees of dieback. The plots were randomly located within stands with abundant dead or defoliated trees delineated by local forest managers. The center of the plot was positioned with a handheld GPS device (spatial uncertainty ca 5 m). In each plot, we identified the species and measured the dbh of all the trees with dbh ≥ 7.5 cm. In these trees, we also evaluated the canopy defoliation as a proxy of forest dieback in classes of 5% following the methodology described in the ICP Forest Manual (ICP Forest, 2016). Defoliation was visually assessed independently by at least two observers to avoid bias. We surveyed crown condition for a total of 2127 trees.

We calculated the mean plot defoliation (DEFOL) weighting the tree defoliation by the dbh, i.e., we used the dbh as a proxy of crown size (Porté et al., 2000). We classified each plot in damage level according to their DEFOL: low (DEFOL < 20%), moderate (20% ≤ DEFOL < 50%) and high (DEFOL ≥ 50%) The mean forest attributes (basal area, tree density and mean plot diameter) by dieback level are shown in Table 1.

We also used the 3-month Standardized Precipitation Evapotranspiration Index (SPEI; https://monitordesequia. csic.es/) at a 1 km^2 resolution to relate forest decay with drought severity over the study period (Vicente-Serrano et al., 2017). Negative values of SPEI indicate a negative water cumulative balance as a function of precipitation and temperature at different time scales (Vicente-Serrano et al., 2010). The weekly and mean annual trends of SPEI are shown in Fig. 2.

2.2. Landsat data processing and vegetation indices estimation

Open access multispectral images from the Landsat archive provided by the United States Geological Survey, accessed through Google Earth

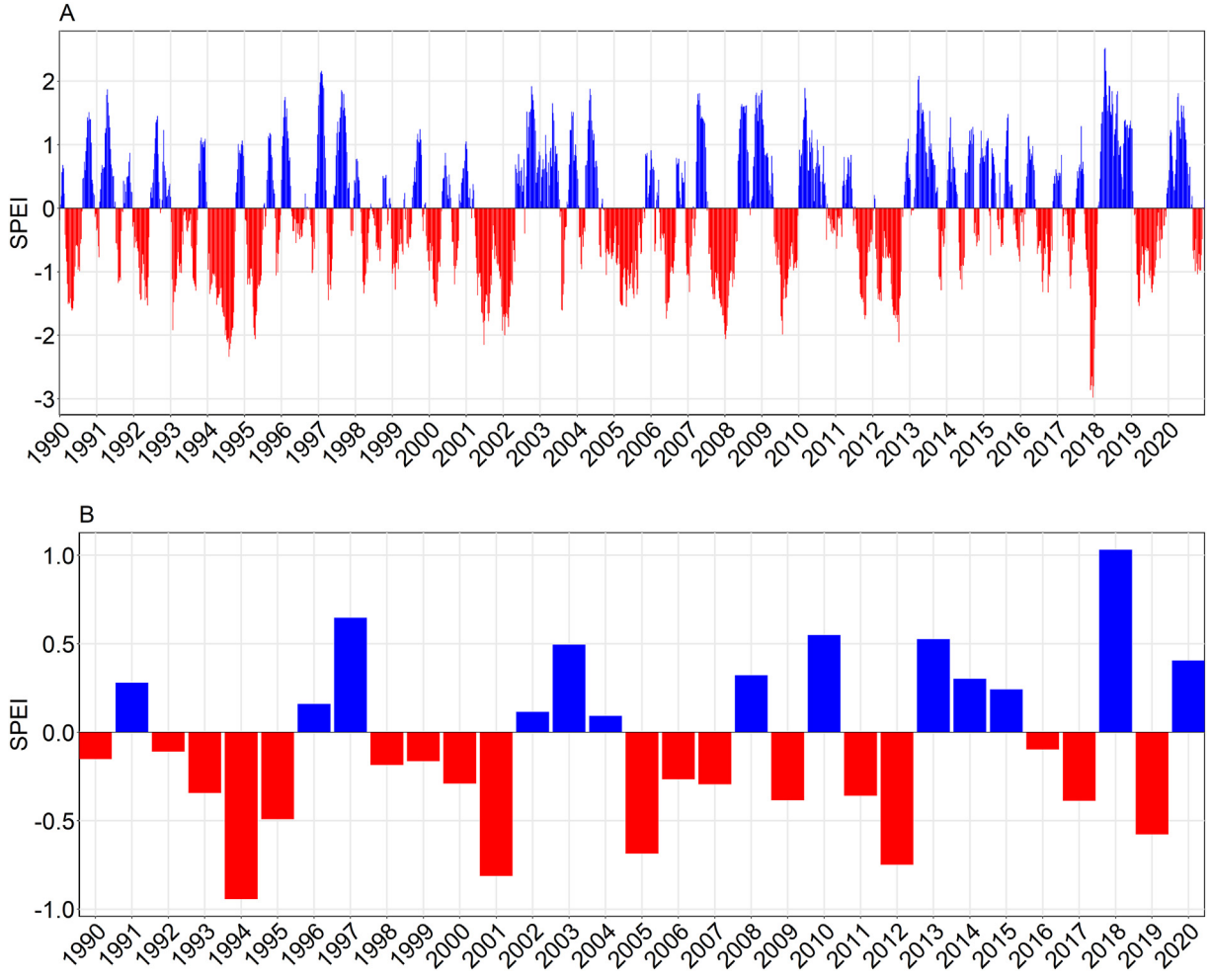

Fig. 2. Three months Standardized Precipitation Evapotranspiration Index (SPEI) from 1962 to 2020. A: Weekly values. B: annual values.

Table 1
Number of plots sampled and characteristics: density, mean diameter at breast height (Dbh), basal area (BA), mean plot defoliation (DEFOL) and percentage of dead trees (Dead). All the values are referred to the trees with Dbh ≥ 7.5 cm. Between brackets the standard deviation.

Variable (units)	Low	Intermediate	High
No. plots	10	17	8
Density (No. trees ha^{-1})	542 (135)	695 (139)	776 (238)
Dbh (cm)	24.1 (6.1)	22.8 (2.7)	20.4 (1.8)
BA (m^2 ha^{-1})	25.7 (7.7)	30.0 (6.9)	28.3 (10.8)
DEFOL (%)	13.1 (6.2)	38.4 (7.9)	57.8 (4.9)
Dead (%)	2.4 (4.4)	7.8 (5.3)	11.1 (7.3)

Engine (GEE), were selected to meet the objectives of this study. To match the field observations with the field plots, we selected those Landsat pixels that included the center of a field plot. We defined the base period for this study to include monthly and cloud-free observations from January 1990 through December 2020. We used GEE to build Landsat time-series, and then applied the topographic correction and inter-sensor harmonization and SIs estimation. Firstly, Tier 1 Surface Reflectance images from Landsat 5 TM, Landsat 7 ETM+ datasets were normalized to Landsat 8 OLI datasets from a multilinear regression approach due to differences between spectral characteristics among sensors (Roy et al., 2016). To remove the effect of the terrain slope we applied the topographic correction SCS + C developed by Soenen et al. (2005), which is based on the Sun-Canopy- Sensor correction (Gu and Gillespie, 1998).

After corrections, monthly composites were generated using a medoid selection process choosing the pixel closest to the median of the corresponding pixels among images (Bright et al., 2019; Flood, 2013). We calculated three greenness vegetation indices: Enhanced Vegetation Index (EVI) (Huete et al., 2002), Normalized Difference Vegetation Index (NDVI) (Tucker, 1979), Soil Adjusted Vegetation Index (SAVI) (Huete, 1988), and two wetness indices: Normalized-Multiband Drought Index (NMDI) (Wilson and Sader, 2002) and Tasseled Cap Wetness (TCW; the coefficients shown below are referred to Landsat 8) (Baig et al., 2014; Hansen et al., 2001a, 2001b) as follows:

$$EVI = G \cdot \frac{(NIR - RED)}{(NIR + C1 \cdot RED - C2 \cdot Blue + L)} \quad (1)$$

$$NDVI = \frac{(NIR - RED)}{(NIR + RED)} \quad (2)$$

$$SAVI = \frac{(NIR - RED)}{(NIR + RED + 0.5)}(1 + 0.5) \quad (3)$$

$$NDMI = \frac{(NIR - SWIR1)}{(NIR + SWIR1)} \quad (4)$$

$$TCW = 0.1511 \cdot Blue + 0.1973 \cdot Green + 0.3283 \cdot Red + 0.3407 \cdot NIR - 0.7117 \cdot SWIR1 - 0.4559 \cdot SWIR2 \quad (5)$$

Whereas EVI, NDVI, SAVI and NDMI are normalized indices ranging between −1 to +1, TCW is a linear combination of six spectral bands. Therefore, the scale for the normalized indices differs from that of TCW. Thus, we multiplied by 1000 normalized indices to obtain similar and comparable values for normalized indices and TCW.

2.3. Decomposition of spectral indices time series and estimation of the phenological metrics

We used the BEAST (Bayesian Estimator of Abrupt change, Seasonal change, and Trend) routine proposed by Zhao et al. (2019b) to decompose plot SIs series into seasonality, trend signal (*Trend*) and noise. This routine consists of an ensemble algorithm that quantifies the relative importance of individual models and uses a Bayesian framework to average these individual models instead of selecting a single best model. BEAST disentangles SI series components and fits linear and nonlinear trends by applying flexible basis functions whereas other algorithms derive only linear or piecewise linear trends (Wang et al., 2011). From an ecological point of view, this algorithm formulation is sound as the underlying environmental processes do not follow purely linear or piecewise-linear patterns over time but rather complex and nonlinear patterns. We refer to Zhao et al. (2019b) for further statistical details of BEAST.

Once plot SIs series were decomposed into their three components, we derived the following phenological metrics from the seasonality component using the approach proposed by White et al. (1997): SOS_{ij}, start of the phenological season (in days of the year, DOY); EOS_{ij}, end of the phenological season (in DOY), $LOS_{ij} = EOS_{ij} - SOS_{ij}$, length of the phenological season (in days), $Peak_{ij}$, maximum value of the phenological season (in SI units); $Trough_{ij}$, minimum value of the phenological season (in SI units), $AMP_{ij} = Peak_{ij} - Trough_{ij}$, peak-to-peak amplitude of the phenological season (in SI units). Subindices *i* and *j* refer to the *i*-th plot (from 1 to 31) and *j*-th month of the time series (from January 1990 to December 2020), respectively. Averaged values per damage level of the metrics for the whole study period are shown in Table 2.

2.4. Statistical analyses

First, we used linear mixed-effects models to determine whether there are any statistically significant differences between the means of six phenological metrics among the three dieback levels. We also aimed to test whether the six phenological metrics followed a temporal pattern over the study period (1990–2020). Then, we fitted 30 models (6 variables × 5 Sis) with the following model formulation:

$$y_{ilk} = Dieback_k + Year_l + Plot_i + \varepsilon_{ilk} \quad (6)$$

where *y* is the value taken by each one of the six variables considered in the year *l* ($l = 1990$ to 2020), *Dieback* is a factor referred to the damage level ($k =$ low, moderate and high) at the gathering data time, *Year* is a covariate, *Plot* is a random effect to account for the intra-plot variability ($i = 1, \ldots, 31$), and ε_{ilk} is the error term (Zuur et al., 2009). The selection of the *Dieback* and *Year* fixed effects was done following a forward stepwise procedure via the likelihood ratio test.

To facilitate the interpretation of the six phenological variables we calculated the z-scores as follows:

$$z = \frac{\left(Phenology_{year} - Phenology_{base}\right)}{\sigma_{base}} \quad (7)$$

where $Phenology_{base}$ and σ_{base} are the mean and standard deviation of the phenological variables for the study period while $Phenology_{year}$ refers to the phenological variables for a given year. Then, we addressed the association between time-lagged of SPEI and the z-scores of the yearly average of the six phenological variables for the five SIs using cross-correlations.

Finally, we used the following additive mixed model (Wood, 2017) to describe the trends of each SI (*Trend*) for the whole period of study of the plots subjected to the three levels of dieback:

$$Trend_{ijk} = Dieback_k + f^k(Time_j) + Plot_i + \varepsilon_{ijk} \quad (8)$$

where $f^k(Time_j)$ is a damage level smoother via thin plate regression splines (Wood, 2003) where the smoothing variable is the *Time* in months. This model formulation allows each damage level to be differently shaped with 95% confidence intervals without restriction, i.e., a measure of the significance of the possible differences of *Trend* among levels of dieback over the study period (Pedersen et al., 2019). The rest of the terms have been defined above. Spatial and temporal autocorrelation of linear and additive mixed models residuals was checked via semivariograms with envelopes after 999 permutations under the

Table 2
Mean values of the metrics derived from the Landsat series by the level of forest dieback and spectral index. Means are calculated for the whole study period (1990–2020). Between brackets the standard deviation. Note that EVI, NDVI, SAVI and NDMI values were multiplied by 1000.

Dieback	*SOS*	*EOS*	*LOS*	*Peak*	*Trough*	*Ampl*	*Trend*
EVI							
High	267.9	76.9	174.0	58.6	−53.0	111.6	502.2
	(6.00)	(7.6)	(3.1)	(9.7)	(8.2)	(17.9)	(59.0)
Moderate	271.8	81.1	173.6	60.7	−54.5	115.2	514.0
	(4.0)	(6.4)	(3.6)	(12.5)	(11.3)	(23.7)	(62.1)
Low	272.8	83.7	176.0	57.6	−53.9	111.5	549.5
	(6.0)	(10.1)	(4.9)	(12.5)	(21.5)	(41.5)	(66.4)
NDVI							
High	262.3	68.6	171.1	49.1	−42.9	92.0	580.6
	(3.1)	(3.6)	(3.0)	(7.6)	(7.4)	(15.0)	(55.6)
Moderate	263.0	71.2	173.0	52.3	−46.0	98.2	595.1
	(4.6)	(5.5)	(4.2)	(8.9)	(7.2)	(15.8)	(57.4)
Low	264.6	73.7	173.8	45.6	−40.6	86.2	625.6
	(9.9)	(9.9)	(4.9)	(13.8)	(12.0)	(25.6)	(62.2)
SAVI							
High	261.9	68.2	171.1	74.2	−64.6	138.8	871.1
	(2.3)	(3.0)	(2.7)	(11.8)	(10.8)	(22.4)	(83.4)
Moderate	263.1	71.3	173.0	78.4	−68.9	147.3	892.4
	(4.6)	(5.4)	(4.2)	(13.6)	(11.3)	(24.5)	(86.0)
Low	264.4	73.6	173.6	68.9	−61.2	130.1	938.5
	(10.0)	(10.8)	(5.3)	(20.4)	(18.3)	(38.4)	(92.6)
NDMI							
High	258.4	57.7	164.0	94.4	−71.7	166.2	260.0
	(4.5)	(3.0)	(4.0)	(21.1)	(19.7)	(40.6)	(89.0)
Moderate	256.7	60.3	168.2	105.6	−84.9	190.5	286.1
	(4.8)	(2.8)	(5.5)	(22.8)	(19.7)	(42)	(74.0)
Low	253.4	61.6	172.7	99.8	−86.7	186.5	328.2
	(7.7)	(7.0)	(5.2)	(14.5)	(16.5)	(30.5)	(79.6)
TCW							
High	253.3	61.2	172.3	245.7	−213.1	458.8	−602.7
	(5.2)	(1.1)	(4.7)	(26.3)	(29.7)	(53.2)	(201.4)
Moderate	251.3	63.0	176.7	255.6	−234.6	490.2	−550.0
	(4.8)	(2.4)	(5.2)	(42.0)	(41.5)	(81.6)	(166.6)
Low	248.5	63.5	179.1	215.4	−204.7	420.0	−450.8
	(5.5)	(4.7)	(2.7)	(29.4)	(27.0)	(56.0)	(163.8)

SOS: start of the phenological season; *EOS*: end of the phenological season, *LOS*: length of the phenological season; *Peak*: maximum value of the phenological season; *Trough*: minimum value of the phenological season; *Ampl*: amplitude of the phenological season; *Trend*: mean value of the trend.

assumption of no spatial correlation (Augustin et al., 2009) and partial autocorrelation plots, respectively.

For this study, we used the following packages implemented in R 4.0.2. environment (R Core Team, 2021): "meteoland" for the data extrapolation from the surrounding climatic stations to the study area (De Cáceres et al., 2018), "Rbeast" for SIs series decomposition (Zhao et al., 2019a), "greenbrown" for the estimation of the seasonal phenological metrics (Forkel et al., 2015), "nlme" for the linear mixed models fitting (Pinheiro et al., 2020) and "mgcv" for the additive mixed models fitting (Wood, 2017).

3. Results

3.1. Relationship between forest attributes and dieback

We found that the plots with different damage levels did not present statistically significant differences ($p > 0.05$) in terms of basal area and mean diameter but plots with high defoliation levels presented higher tree density than the two other levels ($p = 0.014$). Stand basal area aggregates information on both stand density and tree size, and its effect was not statistically significant, suggesting that competition due to higher stand density was not the main defoliation driver during the field survey (2020−2021).

3.2. Land surface phenological metrics over the study period

The visual inspection of the seasonal trajectories revealed unimodal patterns of the phenological season for the three levels of damage regardless of the SI considered (Supplementary material 1). The start of the phenological season took place around the DOY 250–270 (late summer and early autumn) while the phenological season ended around the DOY 60–80 (late winter and early spring) depending on the SI and the damage level (Table 2). The inspection of the Table 2 reveals that both *SOS* and *EOS* occurred some days earlier when considering the wetness indices (NMDI and TCW) than when considering the greenness indices (EVI, NDVI and SAVI). *LOS* spanned ca. 170 days being longer in healthier than in damaged plots. However, from a statistical point of view, the inspection of the models indicates none of the six land surface phenological variables was related to damage level over the study period (Pr(>Chisq) > 0.05; Table 3). As regards the temporal pattern of the six land surface phenological variables, we found that the *SOS* was significantly delayed from 1990 to 2020 when using NDVI and SAVI (positive relationship between *SOS* and *Year* in Table 3) whereas the timing of *SOS* and *EOS* advanced over the study period when using TCW. However, we did not find any statistical evidence of shortening or lengthening of *LOS* over the last 31 years. According to NDVI, SAVI and TCW, *Ampl* extended over the study period because of the elongation of *Peak* and *Trough*. Note that *Trough* takes negative values, therefore, a negative relationship of this variable with *Year* indicates larger values of *Trough* in absolute terms.

The inspection of the z-scores of the six phenological variables indicates that they depicted oscillation over the whole study period without a defined pattern (Supplementary material 2). The cross-correlations between SPEI and the z-scores of the six phenological variables revealed lagged associations. We found negative and 5–7 years lagged relationships between SPEI and *LOS* for NDVI, SAVI and TCW, that may be the

Table 3
Results of the likelihood test (Pr(>Chisq)) for the *Dieback* fixed effect and *Year* covariate (resulting from Eq. (6)). Between brackets the sign of the significant relationship at $\alpha \leq 0.05$.

Period	*SOS*	*EOS*	*LOS*	*Peak*	*Trough*	*Ampl*
Dieback						
EVI	0.3152	0.9685	0.5043	0.7286	0.5990	0.9187
NDVI	0.2200	0.7549	0.3636	0.1897	0.7723	0.4645
SAVI	0.2358	0.7322	0.3279	0.1778	0.8193	0.4630
NDMI	0.8139	0.8848	0.9591	0.8474	0.9730	0.9364
TCW	0.0917	0.9870	0.6548	0.2236	0.6861	0.2444
Year						
EVI	0.3385	0.0997	0.9957	0.4099	0.2751	0.3324
NDVI	0.0176 (+)	0.0856	0.3315	0.0078 (+)	0.0278 (−)	0.0125 (+)
SAVI	0.0206 (+)	0.0499 (+)	0.4022	0.0076 (+)	0.0283 (−)	0.0125 (+)
NDMI	<0.0001 (−)	<0.0001 (−)	0.0751	0.2696	0.9133	0.4909
TCW	0.1273	0.0825	0.7409	0.0189 (+)	0.0717	0.0306 (+)

SOS: start of the phenological season; *EOS*: end of the phenological season, *LOS*: length of the phenological season; *Peak*: maximum value of the phenological season; *Trough*: minimum value of the phenological season; *Ampl*: amplitude of the phenological season.

Table 4
Summary of the cross-correlations between SPEI and the six phenological metrics for the five spectral indices. The number indicates the lags (in years) that each SPEI metric correlation applies to. Negative lagged correlations (phenological event preceded SPEI event) are not shown. Between brackets the sign of the significant relationship at $\alpha \leq 0.05$. n.s. = non-significant relationships.

Index	*SOS*	*EOS*	*LOS*	*Peak*	*Trough*[a]	*Ampl*
EVI	2 (+)	n.s.	n.s.	n.s.	n.s.	n.s.
NDVI	n.s.	n.s.	5 (−)	n.s.	3 (−)	3 (+)
SAVI	n.s.	n.s.	5 (−)	n.s.	3 (−)	3 (+)
NDMI	1 (−)	n.s.	n.s.	n.s.	n.s.	n.s.
TCW	n.s.	n.s.	7 (−)	3 (+)	3 (−)	3 (+)

[a] Note that *Trough* takes negative values and negative correlations between *Trough* and SPEI indicate positive relationships in absolute values. *SOS*: start of the phenological season; *EOS*: end of the phenological season, *LOS*: length of the phenological season; *Peak*: maximum value of the phenological season; *Trough*: minimum value of the phenological season; *Ampl*: amplitude of the phenological season.

result of chance rather than causality (Table 4). The cross-correlations also suggest a positive and 3-year lagged association between SPEI and *Peak* and *Trough* for all the SI except for EVI and TCW, which resulted in similar relationships between SPEI and *Ampl*.

3.3. Spectral indices trends over the study period

We found a significant effect ($p < 0.05$) of the *Dieback* factor and f^k ($Time_j$) on the five SI trends studied here. The smoothing representation of the trends over the study period revealed that the SI trends decreased from 1990 to 1993–1995, regardless of the SI analyzed (Fig. 3). The trends of the three levels of dieback during these years were close and the confidence intervals overlapped, which indicates the lack of significant differences among dieback levels. This drop in the SIs coincides with a period (1993–1995) with the highest number of consecutive years with negative annual SPEI, i.e., dry and warm years, over the monitoring period (Fig. 2B). From this dry period, the smoothed trends for the three levels of dieback increased but, unlike the previous years, the curves separated, displaying the low damage plots the highest SI values while the highest damage level presented the lowest values for the five SIs. High and moderate smoothed trends were relatively close whereas the low curve was distant from the two other curves irrespective of the SI used. Hence, the main statistical differences, i.e., non-overlapping confidence intervals, occurred between the low and high dieback levels.

The trends of the three greenness indices peaked during 2014–2016 whereas the smoothing curves for the two wetness indices reached their maximum in 2006 and then continuously decreased until 2017–2018, reaching similar values or even lower to those of the drought period of 1993–1995. It is worth noting that 2005–2006 was another dry period (Fig. 2B) and that the end of 2017 presented the lowest weekly values of SPEI (Fig. 2A). The *Trend* smoothed patterns also displayed a local minimum in 2009–2011 which also coincides with a dry period according. Despite these minima coincided for the five SIs trends used, the *Trend* of EVI depicted a rougher pattern than the

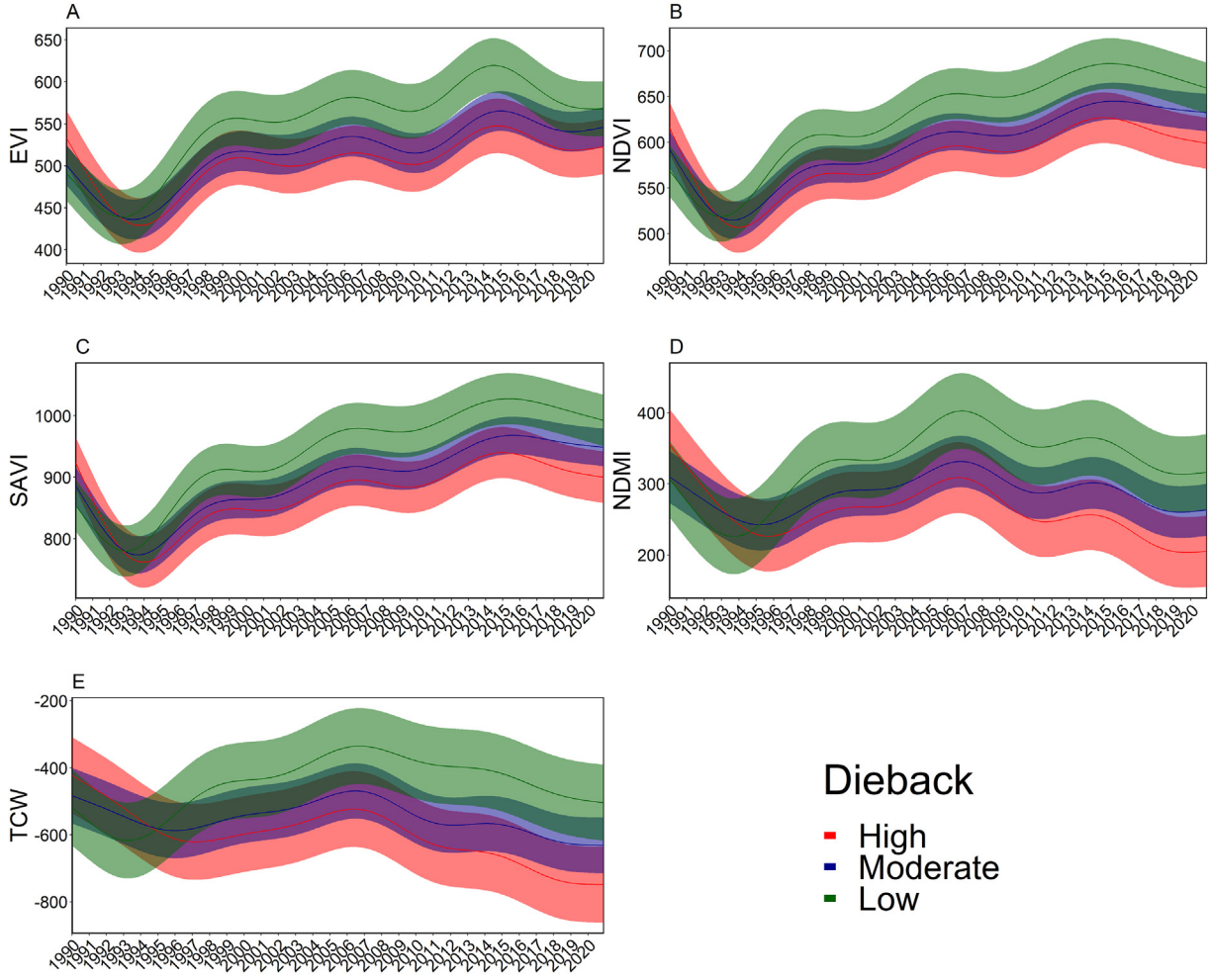

Fig. 3. Smoothed representation (resulting from Eq. (8)) for the five spectral indices over the monitoring period (January 1990 – December 2020) grouped by dieback level. The shaded areas indicate the 95% confidence intervals. Note that EVI, NDVI, SAVI and NDMI values were multiplied by 1000.

other two greenness indices, i.e., the drops in the EVI *Trend* during the dry years were larger than those of NDVI or SAVI. Similarly, the *Trend* of NDWI followed a rough pattern whereas the TCW pattern was more linear.

4. Discussion

4.1. Influence of forest dieback and climate on phenological metrics

Despite being pivotal indicators of climate-vegetation interactions, few studies have addressed the relationship between forest dieback and phenological metrics (SIs) derived from satellite products.

In agreement with previous findings carried out in the Mediterranean region, the satellite-based phenological season for pines starts in winter due to the mild temperatures, high soil moisture and low leaf vapor pressure and reaches the minimum in summer when drought peaks (Aragones et al., 2019; Atzberger et al., 2013; Maseyk et al., 2008; Peñuelas et al., 2004). Accordingly, Calama et al. (2013) found that the minimum values of net photosynthetic assimilation rates for another Mediterranean pine (*Pinus pinea* L.) were reached during the summer as a response to the drought. Under these conditions, the phenological season is not coincident with the canopy and stem growing season, which typically takes place during the spring and the autumn (see Camarero et al. (2010) and Aldea et al. (2017) for *Pinus halepensis* Mill. and *P. pinaster* stem increment patterns, respectively). The minimum values for the SIs found in summer also coincide with the maximum litterfall rates for this species (Espinosa et al., 2018; Roig et al., 2005). The shedding of needles during the summer season has been suggested to be a strategy to cope with drought stress and elevated temperatures (Manzoni et al., 2015). Moreover, the satellite-based phenological season depicts different patterns in other latitudes and groups of tree species where the low winter temperatures (Jin et al., 2013), snow (Kobayashi et al., 2016) as well as the leafing-out and leaves shedding (Muraoka et al., 2013; Polgar and Primack, 2011) reduce or even inhibit the phenological activity. Then, this explains the maximum of the SI plateaus during the spring, summer and autumn for deciduous broadleaves (Ryu et al., 2014) and boreal conifer forests (Kobayashi et al., 2018).

Our results point out that the six phenological metrics have not been impacted by forest dieback although the cross-correlations identified lagged relationships between SPEI and *LOS, Peak, Trough* and *Ampl*. These correlations must be considered with caution. In the study area, *LOS* should be constrained by harsh periods (low rainfall and high temperature) rather than by low temperatures and snowpack during the winter (Recuero et al., 2019; White et al., 2009). Similarly, Ma et al. (2015) found increments in *LOS* during wet years in Southeastern Australia. Several authors point towards a lengthening of the phenological season of the Northern Hemisphere as well as an advance in *SOS* as a consequence of climate change (Jeong et al., 2011; Karkauskaite et al., 2017) although some regions in France, Italy and around the Caspian Sea displayed shortening of the phenological season while the Iberian and Anatolian peninsulas do not show clear patterns (Garonna et al., 2014). Accordingly, our results do not provide any evidence of elongation or shortening patterns of *LOS* over the last 31 years.

Contrary to *EOS, SOS* and *LOS*, the amplitude of the cycles is not widely studied (but see (Aragones et al., 2019; Recuero et al., 2019; van Leeuwen et al., 2010)). With this regard, Recuero et al. (2019) argued that the lowest amplitudes of the seasonality are linked to the lowest yearly NDVI values when analyzing land surface phenological metrics at the global scale. On the other hand, pines from xeric sites display larger amplitudes values than pines species growing in more humid conditions within the Mediterranean regions (Aragones et al., 2019). However, our results have not revealed any statistical evidence of the influence of the dieback on the peak-to-peak amplitude of the seasonality.

4.2. Trend of the spectral indices as early-warning indicators of forest dieback

As expected, our findings indicated that plots with high damage level displayed lower values of the *Trend* of the SIs than healthier plots. Similarly, several authors reported decreases in canopy greenness associated with changes in climatic conditions (Barbosa and Asner, 2017; Zhao et al., 2017) and with insect outbreaks (Sangüesa-Barreda et al., 2014). Hence, our findings revealed that drops in *Trend* tended to occur with harsher years, specifically very dry periods. This was especially evident for the period 1993–1995, which was preceded by some dry years during the 1980s. The period 1993–1995 is recognized to be one of the major droughts periods of the last decades which most negatively impacted tree growth and forest productivity in Spain (Gazol et al., 2018). Since this harsh period, *Trend* for the five SIs followed separated patterns which indicates that the recovery capacity after drought presented spatial heterogeneity. Similarly, Liu et al. (2021) found that the stands with higher canopy recovery capacity after the initial decline depicted higher resilience to climate change in the taiga. The above mentioned spatial heterogeneity could be linked among other factors to soil conditions (soil depth, water holding capacity), stand structure and competition (Marqués et al., 2021) and, probably, to solar radiation exposure although further research is required (see Pérez-Luque et al. (2020)).

The difference among *Trend* smoothed patterns shows the capability of the *Trend* metric as an early warning indicator of forest dieback. Therefore, it seems reasonable to implement remote sensing-based monitoring systems to carry out management measures capable to alleviate the consequences of harsh periods. The *Trend*-related results are in agreement with similar signals obtained through retrospective quantifications of tree-ring width (Camarero et al., 2015a, 2015b) or wood anatomy (Pellizzari et al., 2016) which allow forecasting dieback in declining trees 2–5 decades before the growth decline occurred and the dieback started. Férriz et al. (2021) studied the dieback process in a *P. pinaster* forest located in Central Spain. In concordance with our results, they found that declining trees displayed lower tree-ring growth than healthier trees since the drought of 1995. Such patterns agree with a long-term deterioration of the hydraulic and photosynthetic systems or the inability to uptake soil water in the most affected trees (Körner, 2019). Since the Landsat images and dendrochronology provide information on different growth traits (primary and secondary growth, respectively) at different scales (landscape and tree, respectively), further efforts should be oriented towards combining information on ring-width chronologies with remote sensing time series to study the links of forest dieback with primary and secondary growth at different spatial and temporal scales (Pérez-Luque et al., 2020).

Our findings indicate that the length of the phenological season did not present significant differences between dieback levels and the *Trend* component of the SIs was larger for healthier plots since the dry period 1993–1995. All together points out that the duration of the photosynthetic period does not change between declining and healthier stands but healthier stands depict larger photosynthetic capacity.

Several authors highlighted the role of the understory on the whole system phenological season, especially when the overstory is composed of deciduous species (Ahl et al., 2006; Ryu et al., 2014), although other researchers have not considered the understory stratum (Aragones et al., 2019). In this work, we have not discriminated the signals of understory from those of the overstory because (i) overstory was dominated by evergreen species, consequently, the influence of the understory is expected to be secondary, and (ii) we are not interested in studying the satellite-based phenological seasonality of the *P. pinaster* but seasonal dynamics of the complete forest system suffering different degrees of damage. In this work, we have not discriminated the signals of understory from those of the overstory. Nevertheless, we were interested in the seasonal dynamics of the complete forest system suffering

different degrees of damage rather than the seasonal dynamics of *P. pinaster* alone. Therefore, the influence of understory on the time-series signal, as a result of successional shifts, can also help discriminating the level of damage.

4.3. Spectral indices comparison

Our results point out differences between wetness (NDMI, TCW) and greenness indices (EVI, NDVI, SAVI), particularly, in regards to the metrics related to the phenological season (start, end and length). Wetness-related indices showed an earlier beginning and end of the season as well as shorter *LOS* as compared to greenness indices. Furthermore, the maximum of *Trend* and, therefore, the last drop in *Trend* took place earlier for wetness than for greenness. The water use strategies of conifers also allow explaining the more pronounced decreasing trends in water wetness (Liu et al., 2021). In contrast to broad-leaved species, which can use the heartwood water, conifers keep their water reserves mainly by real-time absorption (Goldsmith, 2013; Querejeta et al., 2007). Therefore, drought periods result in drops in canopy water content while sustained water deficit may reduce the photosynthetic activity, and, consequently the canopy greenness (Liu et al., 2021). This suggests that the amount of water is an earlier indicator of forest dieback than pigment concentration and, consequently, that wetness indices react earlier to vegetation decline, making them more suitable early-warning signals. Indeed, recent investigations recommend using wetness indices to monitor forest decline as this type of indices are more related to physiological variables (e.g., water potential, hydraulic conductivity and capacitance) than greenness indices (Marusig et al., 2020).

5. Conclusions

The potential of metrics derived from long time series of Landsat-based spectral indices to characterize forest dieback has been demonstrated. The dieback process in the study *P. pinaster* forest is mainly reflected in the *Trend* component of the spectral indices series, whereas our results revealed no significant relationship between the dieback and the land surface phenological metrics (that is, the seasonal component of the spectral indices). Wetness indices showed an earlier response to drought than greenness indices making them suitable to forecast drought-triggered dieback.

The *Trend* component dropped in 1993–1995, about 25 years before the dieback started in 2017. After this initial drop, trajectories of SIs for different levels of dieback showed a distinct evolution, making them distinguishable from each other, particularly between low and high dieback levels. The *Trend* component of wetness indices also showed higher sensitivity to subsequent droughts in 2004–2005. Therefore, in concordance with our results, we recommend using this metric derived from wetness indices as a potential early warning signal of forest dieback as well as a useful tool to detect areas prone to suffer dieback and to implement management measures (e.g., reduction of competition through thinning) capable to buffer the negative impacts of drought.

Supplementary data to this article can be found online at https://doi.org/10.1016/j.scitotenv.2021.148578.

Declaration of competing interest

The authors declare that they have no known competing financial interests or personal relationships that could have appeared to influence the work reported in this paper.

Acknowledgments

DMF is supported by the Spanish Ministry of Science through the Juan de la Cierva Formación post-doctoral program (FJC2018-037870-I). AVS is supported by the Ministry of Science, Innovation and Universities through a FPU pre-doctoral fellowship (FPU17/03260). We acknowledge the critical input of forest managers (Aragón Regional Govt.) Álvaro Hernández and Enrique Arrechea, in identifying critical areas, providing natural and management history details and supporting our activities. We thank the Spanish Agency of Meteorology for the open-access climatic data availability. We acknowledge support from grants DARE (RTI2018-096884-B-C32), and FORMAL (RTI2018-096884-B-C31) funded by the Spanish Ministry of Science, Innovation and Universities. We also thank the two anonymous reviewers for their comments.

CRediT authorship contribution statement

D. M-F.: Statistical analysis, Writing - original draft preparation. **A. V—S.**: processing of GEE data, Writing - Reviewing & Editing. **JJ. C.**: Writing - Reviewing & Editing, Funding Acquisition. **M.A. Z.:** Writing - Reviewing & Editing, Funding Acquisition. **J. T:** data gathering, Resources, Editing. **M. G.:** Writing - Reviewing & Editing, Funding Acquisition, Conceptualization, Methodology.

References

Ahl, D.E., Gower, S.T., Burrows, S.N., Shabanov, N.V., Myneni, R.B., Knyazikhin, Y., 2006. Monitoring spring canopy phenology of a deciduous broadleaf forest using MODIS. Remote Sens. Environ. 104, 88–95. https://doi.org/10.1016/j.rse.2006.05.003.

Aitken, S.N., Yeaman, S., Holliday, J.a., Wang, T., Curtis-McLane, S., 2008. Adaptation, migration or extirpation: climate change outcomes for tree populations. Evol. Appl. 1, 95–111. https://doi.org/10.1111/j.1752-4571.2007.00013.x.

Aldea, J., Bravo, F., Bravo-Oviedo, A., Ruiz-Peinado, R., Rodríguez, F., del Río, M., 2017. Thinning enhances the species-specific radial increment response to drought in Mediterranean pine-oak stands. Agric. For. Meteorol. 237, 371–383. https://doi.org/10.1016/j.agrformet.2017.02.009.

Allen, C.D., Macalady, A.K., Chenchouni, H., Bachelet, D., McDowell, N., Vennetier, M., Kitzberger, T., Rigling, A., Breshears, D.D., Hogg, E.H. (Ted), Gonzalez, P., Fensham, R., Zhang, Z., Castro, J., Demidova, N., Lim, J.-H., Allard, G., Running, S.W., Semerci, A., Cobb, N., 2010. A global overview of drought and heat-induced tree mortality reveals emerging climate change risks for forests. For. Ecol. Manag. 259, 660–684. https://doi.org/10.1016/J.FORECO.2009.09.001.

Allen, C.D., Breshears, D.D., McDowell, N.G., 2015. On underestimation of global vulnerability to tree mortality and forest die-off from hotter drought in the Anthropocene. Ecosphere 6, 129. https://doi.org/10.1890/ES15-00203.1.

Anderegg, W.R.L., Kane, J.M., Anderegg, L.D.L., 2013. Consequences of widespread tree mortality triggered by drought and temperature stress. Nat. Clim. Chang. https://doi.org/10.1038/nclimate1635.

Anderegg, W.R.L., Hicke, J.A., Fisher, R.A., Allen, C.D., Aukema, J., Bentz, B., Hood, S., Lichstein, J.W., Macalady, A.K., McDowell, N., Pan, Y., Raffa, K., Sala, A., Shaw, J.D., Stephenson, N.L., Tague, C., Zeppel, M., 2015. Tree mortality from drought, insects, and their interactions in a changing climate. New Phytol. 208, 674–683. https://doi.org/10.1111/nph.13477.

Anderegg, W.R.L., Anderegg, L.D.L., Huang, C. ying, 2019. Testing early warning metrics for drought-induced tree physiological stress and mortality. Glob. Chang. Biol. 25, 2459–2469. https://doi.org/10.1111/gcb.14655.

Aragones, D., Rodriguez-Galiano, V.F., Caparros-Santiago, J.A., Navarro-Cerrillo, R.M., 2019. Could land surface phenology be used to discriminate Mediterranean pine species? Int. J. Appl. Earth Obs. Geoinf. 78, 281–294. https://doi.org/10.1016/j.jag.2018.11.003.

Assal, T.J., Anderson, P.J., Sibold, J., 2016. Spatial and temporal trends of drought effects in a heterogeneous semi-arid forest ecosystem. For. Ecol. Manag. 365, 137–151. https://doi.org/10.1016/j.foreco.2016.01.017.

Atzberger, C., Klisch, A., Mattiuzzi, M., Vuolo, F., 2013. Phenological Metrics Derived over the European Continent from NDVI3g Data and MODIS Time Series. Remote Sens. 6, 257–284. https://doi.org/10.3390/rs6010257.

Augustin, N.H., Musio, M., von Wilpert, K., Kublin, E., Wood, S.N., Schumacher, M., 2009. Modeling spatiotemporal forest health monitoring data. J. Am. Stat. Assoc. 104, 899–911. https://doi.org/10.1198/jasa.2009.ap07058.

Baig, M.H.A., Zhang, L., Shuai, T., Tong, Q., 2014. Derivation of a tasselled cap transformation based on Landsat 8 at-satellite reflectance. Remote Sens. Lett. 5, 423–431. https://doi.org/10.1080/2150704X.2014.915434.

Barbosa, J.M., Asner, G.P., 2017. Effects of long-term rainfall decline on the structure and functioning of Hawaiian forests. Environ. Res. Lett. 12. https://doi.org/10.1088/1748-9326/aa7ee4.

Bell, D.M., Cohen, W.B., Reilly, M., Yang, Z., 2018. Visual interpretation and time series modeling of Landsat imagery highlight drought's role in forest canopy declines. Ecosphere 9. https://doi.org/10.1002/ecs2.2195.

Bonfils, C.J.W., Santer, B.D., Fyfe, J.C., Marvel, K., Phillips, T.J., Zimmerman, S.R.H., 2020. Human influence on joint changes in temperature, rainfall and continental aridity. Nat. Clim. Chang. 10, 726–731. https://doi.org/10.1038/s41558-020-0821-1.

Bright, B.C., Hudak, A.T., Kennedy, R.E., Braaten, J.D., Henareh Khalyani, A., 2019. Examining post-fire vegetation recovery with Landsat time series analysis in three western North American forest types. Fire Ecol. 15, 8. https://doi.org/10.1186/s42408-018-0021-9.

Byer, S., Jin, Y., 2017. Detecting drought-induced tree mortality in Sierra Nevada forests with time series of satellite data. Remote Sens. 9, 14–17. https://doi.org/10.3390/rs9090929.

Cailleret, M., Jansen, S., Robert, E.M.R., Desoto, L., Aakala, T., Antos, J.A., Beikircher, B., Bigler, C., Bugmann, H., Caccianiga, M., Čada, V., Camarero, J.J., Cherubini, P., Cochard, H., Coyea, M.R., Čufar, K., Das, A.J., Davi, H., Delzon, S., Dorman, M., Gea-Izquierdo, G., Gillner, S., Haavik, L.J., Hartmann, H., Hereş, A., Hultine, K.R., Janda, P., Kane, J.M., Kharuk, V.I., Kitzberger, T., Klein, T., Kramer, K., Lens, F., Levanic, T., Linares Calderon, J.C., Lloret, F., Lobo-Do-Vale, R., Lombardi, F., López Rodríguez, R., Mäkinen, H., Mayr, S., Mészáros, I., Metsaranta, J.M., Minunno, F., Oberhuber, W., Papadopoulos, A., Peltoniemi, M., Petritan, A.M., Rohner, B., Sangüesa-Barreda, G., Sarris, D., Smith, J.M., Stan, A.B., Sterck, F., Stojanović, D.B., Suarez, M.L., Svoboda, M., Tognetti, R., Torres-Ruiz, J.M., Trotsiuk, V., Villalba, R., Vodde, F., Westwood, A.R., Wyckoff, P.H., Zafirov, N., Martínez-Vilalta, J., 2017. A synthesis of radial growth patterns preceding tree mortality. Glob. Chang. Biol. 23, 1675–1690. https://doi.org/10.1111/gcb.13535.

Calama, R., Puértolas, J., Madrigal, G., Pardos, M., 2013. Modeling the environmental response of leaf net photosynthesis in *Pinus pinea* L. natural regeneration. Ecol. Model. 251, 9–21. https://doi.org/10.1016/j.ecolmodel.2012.11.029.

Camarero, J.J., Olano, J.M., Parras, A., 2010. Plastic bimodal xylogenesis in conifers from continental Mediterranean climates. New Phytol. 185, 471–480. https://doi.org/10.1111/j.1469-8137.2009.03073.x.

Camarero, J.J., Franquesa, M., Sangüesa-Barreda, G., 2015a. Timing of drought triggers distinct growth responses in holm oak: implications to predict warming-induced forest defoliation and growth decline. Forests 6, 1576–1597. https://doi.org/10.3390/f6051576.

Camarero, Julio J., Gazol, A., Sangüesa-Barreda, G., Oliva, J., Vicente-Serrano, S.M., 2015b. To die or not to die: early warnings of tree dieback in response to a severe drought. J. Ecol. 103, 44–57. https://doi.org/10.1111/1365-2745.12295.

Camarero, J.J., Guada, G., Sánchez-Salguero, R., Cervantes, E., 2016. Winter drought impairs xylem phenology, anatomy and growth in Mediterranean Scots pine forests. Tree Physiol. 36, 1536–1549. https://doi.org/10.1093/treephys/tpw077.

Campbell, M.J., Dennison, P.E., Tune, J.W., Kannenberg, S.A., Kerr, K.L., Codding, B.F., Anderegg, W.R.L., 2020. A multi-sensor, multi-scale approach to mapping tree mortality in woodland ecosystems. Remote Sens. Environ. 245, 111853. https://doi.org/10.1016/j.rse.2020.111853.

Chakraborty, A., Seshasai, M.V.R., Reddy, C.S., Dadhwal, V.K., 2018. Persistent negative changes in seasonal greenness over different forest types of India using MODIS time series NDVI data (2001–2014). Ecol. Indic. 85, 887–903. https://doi.org/10.1016/j.ecolind.2017.11.032.

Chen, L., Huang, J., Dawson, A., Zhai, L., Stadt, K.J., Comeau, P.G., Whitehouse, C., 2018. Contributions of insects and droughts to growth decline of trembling aspen mixed boreal forest of western Canada. Glob. Chang. Biol. 24, 655–667. https://doi.org/10.1111/gcb.13855.

de la Cruz, A.C., Gil, P.M., Fernández-Cancio, Á., Minaya, M., Navarro-Cerrillo, R.M., Sánchez-Salguero, R., Grau, J.M., 2014. Defoliation triggered by climate induced effects in Spanish ICP Forests monitoring plots. For. Ecol. Manag. 331, 245–255. https://doi.org/10.1016/j.foreco.2014.08.010.

De Cáceres, M., Martin-StPaul, N., Turco, M., Cabon, A., Granda, V., 2018. Estimating daily meteorological data and downscaling climate models over landscapes. Environ. Model. Softw. 108, 186–196. https://doi.org/10.1016/j.envsoft.2018.08.003.

Earles, J.M., Stevens, J.T., Sperling, O., Orozco, J., North, M.P., Zwieniecki, M.A., 2018. Extreme mid-winter drought weakens tree hydraulic-carbohydrate systems and slows growth. New Phytol. 219, 89–97. https://doi.org/10.1111/nph.15136.

Espinosa, J., Madrigal, J., De La Cruz, A.C., Guijarro, M., Jimenez, E., Hernando, C., 2018. Short-term effects of prescribed burning on litterfall biomass in mixed stands of *Pinus nigra* and *Pinus pinaster* and pure stands of Pinus nigra in the Cuenca Mountains (Central-Eastern Spain). Sci. Total Environ. 618, 941–951. https://doi.org/10.1016/j.scitotenv.2017.08.291.

Férriz, M., Martin-Benito, D., Cañellas, I., Gea-Izquierdo, G., 2021. Sensitivity to water stress drives differential decline and mortality dynamics of three co-occurring conifers with different drought tolerance. For. Ecol. Manag. 486, 118964. https://doi.org/10.1016/j.foreco.2021.118964.

Flood, N., 2013. Seasonal composite Landsat TM/ETM+ images using the medoid (a multi-dimensional median). Remote Sens. 5, 6481–6500. https://doi.org/10.3390/rs5126481.

Forkel, M., Migliavacca, M., Thonicke, K., Reichstein, M., Schaphoff, S., Weber, U., Carvalhais, N., 2015. Codominant water control on global interannual variability and trends in land surface phenology and greenness. Glob. Chang. Biol. 21, 3414–3435. https://doi.org/10.1111/gcb.12950.

Gao, X., Giorgi, F., 2008. Increased aridity in the Mediterranean region under greenhouse gas forcing estimated from high resolution simulations with a regional climate model. Glob. Planet. Chang. 62, 195–209. https://doi.org/10.1016/j.gloplacha.2008.02.002.

Garonna, I., de Jong, R., de Wit, A.J.W., Mücher, C.A., Schmid, B., Schaepman, M.E., 2014. Strong contribution of autumn phenology to changes in satellite-derived growing season length estimates across Europe (1982-2011). Glob. Chang. Biol. 20, 3457–3470. https://doi.org/10.1111/gcb.12625.

Gazol, A., Camarero, J.J., Vicente-Serrano, S.M., Sánchez-Salguero, R., Gutiérrez, E., de Luis, M., Sangüesa-Barreda, G., Novak, K., Rozas, V., Tíscar, P.A., Linares, J.C., Martín-Hernández, N., Martínez del Castillo, E., Ribas, M., García-González, I., Silla, F., Camisón, A., Génova, M., Olano, J.M., Longares, L.A., Hevia, A., Tomás-Burguera, M., Galván, J.D., 2018. Forest resilience to drought varies across biomes. Glob. Chang. Biol. 24, 2143–2158. https://doi.org/10.1111/gcb.14082.

Gazol, A., Sangüesa-Barreda, G., Camarero, J.J., 2020. Forecasting forest vulnerability to drought in Pyrenean silver fir forests showing dieback. Front. For. Glob. Chang. 3, 1–13. https://doi.org/10.3389/ffgc.2020.00036.

Giorgi, F., Lionello, P., 2008. Climate change projections for the Mediterranean region. Glob. Planet. Chang. 63, 90–104. https://doi.org/10.1016/j.gloplacha.2007.09.005.

Goldsmith, G.R., 2013. Changing directions: the atmosphere-plant-soil continuum. New Phytol. 199, 4–6. https://doi.org/10.1111/nph.12332.

Gu, D., Gillespie, A., 1998. Topographic normalization of Landsat TM images of forest based on subpixel Sun-canopy-sensor geometry. Remote Sens. Environ. 64, 166–175. https://doi.org/10.1016/S0034-4257(97)00177-6.

Hamunyela, E., Verbesselt, J., Herold, M., 2016. Using spatial context to improve early detection of deforestation from Landsat time series. Remote Sens. Environ. 172, 126–138. https://doi.org/10.1016/j.rse.2015.11.006.

Hansen, A.J., Neilson, R.P., Dale, V.H., Flather, C.H., Iverson, L.R., Currie, D.J., Shafer, S., Cook, R., Bartlein, P.J., 2001a. Global change in forests: responses of species, communities and biomes. Bioscience 51, 765–779. https://doi.org/10.1641/0006-3568(2001)051[0765:GCIFRO]2.0.CO;2.

Hansen, M.J., Franklin, S.E., Woudsma, C., Peterson, M., 2001b. Forest structure classification in the North Columbia mountains using the Landsat TM Tasseled Cap wetness component. Can. J. Remote. Sens. 27, 20–32. https://doi.org/10.1080/07038992.2001.10854916.

Huete, A.R., 1988. A soil-adjusted vegetation index (SAVI). Remote Sens. Environ. 25, 295–309. https://doi.org/10.1016/0034-4257(88)90106-X.

Huete, A., Didan, K., Miura, T., Rodriguez, E.P., Gao, X., Ferreira, L.G., 2002. Overview of the radiometric and biophysical performance of the MODIS vegetation indices. Remote Sens. Environ. 83, 195–213. https://doi.org/10.1016/S0034-4257(02)00096-2.

ICP Forest, 2016. International Co-operative Programme on Assessment and Monitoring of Air Pollution Effects on Forests.

Jeong, S.J., Ho, C.H., Gim, H.J., Brown, M.E., 2011. Phenology shifts at start vs. end of growing season in temperate vegetation over the Northern Hemisphere for the period 1982-2008. Glob. Chang. Biol. 17, 2385–2399. https://doi.org/10.1111/j.1365-2486.2011.02397.x.

Jiao, T., Williams, C.A., Rogan, J., De Kauwe, M.G., Medlyn, B.E., 2020. Drought impacts on Australian vegetation during the millennium drought measured with multisource spaceborne remote sensing. J. Geophys. Res. Biogeosci. 125, e2019JG005145. https://doi.org/10.1029/2019JG005145.

Jin, Z., Zhuang, Q., He, J.S., Luo, T., Shi, Y., 2013. Phenology shift from 1989 to 2008 on the Tibetan Plateau: an analysis with a process-based soil physical model and remote sensing data. Clim. Chang. 119, 435–449. https://doi.org/10.1007/s10584-013-0722-7.

Karkauskaite, P., Tagesson, T., Fensholt, R., 2017. Evaluation of the Plant Phenology Index (PPI), NDVI and EVI for start-of-season trend analysis of the northern hemisphere boreal zone. Remote Sens. 9, 485. https://doi.org/10.3390/rs9050485.

Kobayashi, H., Yunus, A.P., Nagai, S., Sugiura, K., Kim, Y., Van Dam, B., Nagano, H., Zona, D., Harazono, Y., Bret-Harte, M.S., Ichii, K., Ikawa, H., Iwata, H., Oechel, W.C., Ueyama, M., Suzuki, R., 2016. Latitudinal gradient of spruce forest understory and tundra phenology in Alaska as observed from satellite and ground-based data. Remote Sens. Environ. 177, 160–170. https://doi.org/10.1016/j.rse.2016.02.020.

Kobayashi, H., Nagai, S., Kim, Y., Yang, W., Ikeda, K., Ikawa, H., Nagano, H., Suzuki, R., 2018. In situ observations reveal how spectral reflectance responds to growing season phenology of an open evergreen forest in Alaska. Remote Sens. 10, 1071. https://doi.org/10.3390/rs10071071.

Körner, C., 2019. Commentary No need for pipes when the well is dry-a comment on hydraulic failure in trees. Tree Physiol. 39, 695–700. https://doi.org/10.1093/treephys/tpz030.

Lebourgeois, F., Rathgeber, C.B.K., Ulrich, E., 2010. Sensitivity of French temperate coniferous forests to climate variability and extreme events (*Abies alba*, *Picea abies* and *Pinus sylvestris*). J. Veg. Sci. 21, 364–376. https://doi.org/10.1111/j.1654-1103.2009.01148.x.

Lebourgeois, F., Gomez, N., Pinto, P., Mérian, P., 2013. Mixed stands reduce *Abies alba* tree-ring sensitivity to summer drought in the Vosges mountains, western Europe. For. Ecol. Manag. 303, 61–71. https://doi.org/10.1016/j.foreco.2013.04.003.

van Leeuwen, W.J.D., Davison, J.E., Casady, G.M., Marsh, S.E., 2010. Phenological characterization of desert sky island vegetation communities with remotely sensed and climate time series data. Remote Sens. 2, 388–415. https://doi.org/10.3390/rs2020388.

Liu, F., Liu, H., Xu, C., Shi, L., Zhu, X., Qi, Y., He, W., 2021. Old-growth forests show low canopy resilience to droughts at the southern edge of the taiga. Glob. Chang. Biol. https://doi.org/10.1111/gcb.15605.

Ma, X., Huete, A., Moran, S., Ponce-Campos, G., Eamus, D., 2015. Abrupt shifts in phenology and vegetation productivity under climate extremes. J. Geophys. Res. Biogeosci. 120, 2036–2052. https://doi.org/10.1002/2015JG003144.

Manion, P., 1981. Tree Disease Concepts. Prentice-Hall, Upper Saddle River, NJ, USA.

Manzoni, S., Vico, G., Thompson, S., Beyer, F., Weih, M., 2015. Contrasting leaf phenological strategies optimize carbon gain under droughts of different duration. Adv. Water Resour. 84, 37–51. https://doi.org/10.1016/j.advwatres.2015.08.001.

Marqués, L., Camarero, J.J., Zavala, M.A., Stoffel, M., Ballesteros-Cánovas, J.A., Sancho-García, C., Madrigal-González, J., 2021. Evaluating tree-to-tree competition during stand development in a relict Scots pine forest: how much does climate matter? Trees - Struct. Funct. https://doi.org/10.1007/s00468-021-02109-8.

Marusig, D., Petruzzellis, F., Tomasella, M., Napolitano, R., Altobelli, A., Nardini, A., 2020. Correlation of field-measured and remotely sensed plant water status as a tool to monitor the risk of drought-induced forest decline. Forests, 11 https://doi.org/10.3390/f11010077.

Maseyk, K., Lin, T., Rotenberg, E., Grünzweig, J., Schwartz, A., Yakir, D., 2008. Physiology – phenology interactions in a productive semi-arid pine forest. New Phytol. 178, 603–616. https://doi.org/10.1111/j.1469-8137.2008.02391.x.

Moreno-Fernández, D., Ledo, A., Martín-Benito, D., Cañellas, I., Gea-Izquierdo, G., 2019. Negative synergistic effects of land-use legacies and climate drive widespread oak

decline in evergreen Mediterranean open woodlands. For. Ecol. Manag. 432, 884–894. https://doi.org/10.1016/j.foreco.2018.10.023.
Móricz, N., Garamszegi, B., Rasztovits, E., Bidló, A., Horváth, A., Jagicza, A., Illés, G., Vekerdy, Z., Somogyi, Z., Gálos, B., 2018. Recent drought-induced vitality decline of black pine (*Pinus nigra* Arn.) in South-West Hungary—is this drought-resistant species under threat by climate change? Forests 9, 414. https://doi.org/10.3390/f9070414.
Muraoka, H., Noda, H.M., Nagai, S., Motohka, T., Saitoh, T.M., Nasahara, K.N., Saigusa, N., 2013. Spectral vegetation indices as the indicator of canopy photosynthetic productivity in a deciduous broadleaf forest. J. Plant Ecol. 6, 393–407. https://doi.org/10.1093/jpe/rts037.
Pedersen, E.J., Miller, D.L., Simpson, G.L., Ross, N., 2019. Hierarchical generalized additive models in ecology: an introduction with mgcv. PeerJ, 2019 https://doi.org/10.7717/peerj.6876.
Pellizzari, E., Camarero, J.J., Gazol, A., Sangüesa-Barreda, G., Carrer, M., 2016. Wood anatomy and carbon-isotope discrimination support long-term hydraulic deterioration as a major cause of drought-induced dieback. Glob. Chang. Biol. 22, 2125–2137. https://doi.org/10.1111/gcb.13227.
Peñuelas, J., Filella, I., Zhang, X., Llorens, L., Ogaya, R., Lloret, F., Comas, P., Estiarte, M., Terradas, J., 2004. Complex spatiotemporal phenological shifts as a response to rainfall changes. New Phytol. 161, 837–846. https://doi.org/10.1111/j.1469-8137.2004.01003.x.
Pérez-Luque, A.J., Gea-Izquierdo, G., Zamora, R., 2020. Land-Use Legacies and Climate Change as a Double Challenge to Oak Forest. Mismatches of Geographical and Ecological Rear Edges. Ecosystems, Resilience https://doi.org/10.1007/s10021-020-00547-y.
Pinheiro, J., Bates, D., DebRoy, S., Sarkar, D., Core Team, R., 2020. nlme: Linear and Nonlinear Mixed Effects Models. R Package Version 3.1-149.
Polgar, C.A., Primack, R.B., 2011. Leaf-out phenology of temperate woody plants: from trees to ecosystems. New Phytol. 191, 926–941. https://doi.org/10.1111/j.1469-8137.2011.03803.x.
Porté, A., Bosc, A., Champion, I., Loustau, D., 2000. Estimating the foliage area of Maritime pine (*Pinus pinaster* Ait.) branches and crowns with application to modelling the foliage area distribution in the crown. Ann. For. Sci. 57, 73–86. https://doi.org/10.1051/forest:2000110.
Pretzsch, H., Grams, T., Häberle, K.H., Pritsch, K., Bauerle, T., Rötzer, T., 2020. Growth and mortality of Norway spruce and European beech in monospecific and mixed-species stands under natural episodic and experimentally extended drought. Results of the KROOF throughfall exclusion experiment. Trees - Struct. Funct. 34, 957–970. https://doi.org/10.1007/s00468-020-01973-0.
Prieto-Recio, C., Martín-García, J., Bravo, F., Diez, J.J., 2015. Unravelling the associations between climate, soil properties and forest management in *Pinus pinaster* decline in the Iberian Peninsula. For. Ecol. Manag. 356, 74–83. https://doi.org/10.1016/j.foreco.2015.07.033.
Querejeta, J.I., Estrada-Medina, H., Allen, M.F., Jiménez-Osornio, J.J., 2007. Water source partitioning among trees growing on shallow karst soils in a seasonally dry tropical climate. Oecologia 152, 26–36. https://doi.org/10.1007/s00442-006-0629-3.
R Core Team, 2021. R: A language and environment for statistical computing.
Recuero, L., Litago, J., Pinzón, J.E., Huesca, M., Moyano, M.C., Palacios-Orueta, A., 2019. Mapping periodic patterns of global vegetation based on spectral analysis of NDVI time series. Remote Sens. 11, 1–21. https://doi.org/10.3390/rs11212497.
Rogers, B.M., Solvik, K., Hogg, E.H., Ju, J., Masek, J.G., Michaelian, M., Berner, L.T., Goetz, S.J., 2018. Detecting early warning signals of tree mortality in boreal North America using multiscale satellite data. Glob. Chang. Biol. 24, 2284–2304. https://doi.org/10.1111/gcb.14107.
Roig, S., Del Río, M., Cañellas, I., Montero, G., 2005. Litter fall in Mediterranean Pinus pinaster Ait. stands under different thinnings regimes. For. Ecol. Manag. 206, 179–190. https://doi.org/10.1016/j.foreco.2004.10.068.
Roy, D.P., Kovalskyy, V., Zhang, H.K., Vermote, E.F., Yan, L., Kumar, S.S., Egorov, A., 2016. Characterization of Landsat-7 to Landsat-8 reflective wavelength and normalized difference vegetation index continuity. Remote Sens. Environ. 185, 57–70. https://doi.org/10.1016/j.rse.2015.12.024.
Ryu, Y., Lee, G., Jeon, S., Song, Y., Kimm, H., 2014. Monitoring multi-layer canopy spring phenology of temperate deciduous and evergreen forests using low-cost spectral sensors. Remote Sens. Environ. 149, 227–238. https://doi.org/10.1016/j.rse.2014.04.015.
Sangüesa-Barreda, G., Camarero, J.J., García-Martín, A., Hernández, R., De la Riva, J., 2014. Remote-sensing and tree-ring based characterization of forest defoliation and growth loss due to the Mediterranean pine processionary moth. For. Ecol. Manag. 320, 171–181. https://doi.org/10.1016/j.foreco.2014.03.008.
Seidl, R., Thom, D., Kautz, M., Martin-Benito, D., Peltoniemi, M., Vacchiano, G., Wild, J., Ascoli, D., Petr, M., Honkaniemi, J., Lexer, M.J., Trotsiuk, V., Mairota, P., Svoboda, M., Fabrika, M., Nagel, T.A., Reyer, C.P.O., 2017. Forest disturbances under climate change. Nat. Clim. Chang. 7, 395–402. https://doi.org/10.1038/nclimate3303.
Simler-Williamson, A.B., Rizzo, D.M., Cobb, R.C., 2019. Interacting effects of global change on forest pest and pathogen dynamics. Annu. Rev. Ecol. Evol. Syst. 50, 381–403. https://doi.org/10.1146/annurev-ecolsys-110218-024934.
Soenen, S.A., Peddle, D.R., Coburn, C.A., 2005. SCS+C: a modified sun-canopy-sensor topographic correction in forested terrain. IEEE Trans. Geosci. Remote Sens. 43, 2148–2159. https://doi.org/10.1109/TGRS.2005.852480.
Stöckli, R., Vidale, P.L., 2004. European plant phenology and climate as seen in a 20-year AVHRR land-surface parameter dataset. Int. J. Remote Sens. 25, 3303–3330. https://doi.org/10.1080/01431160310001618149.
Trumbore, S., Brando, P., Hartmann, H., 2015. Forest health and global change. Science https://doi.org/10.1126/science.aac6759.
Tucker, C.J., 1979. Red and photographic infrared linear combinations for monitoring vegetation. Remote Sens. Environ. 8, 127–150. https://doi.org/10.1016/0034-4257(79)90013-0.
Turco, M., Ceglar, A., Prodhomme, C., Soret, A., Toreti, A., Francisco, J.D.-R., 2017. Summer drought predictability over Europe: empirical versus dynamical forecasts. Environ. Res. Lett. 12, 84006. https://doi.org/10.1088/1748-9326/aa7859.
Valbuena-Carabaña, M., de Heredia, U.L., Fuentes-Utrilla, P., González-Doncel, I., Gil, L., 2010. Historical and recent changes in the Spanish forests: a socio-economic process. Rev. Palaeobot. Palynol. 162, 492–506. https://doi.org/10.1016/j.revpalbo.2009.11.003.
Varo-Martínez, M., Navarro-Cerrillo, R.M., 2021. Stand delineation of *Pinus sylvestris* L. plantations suffering decline processes based on biophysical tree crown variables: a necessary tool for adaptive silviculture. Forests 13, 436.
Verbesselt, J., Hyndman, R., Newnham, G., Culvenor, D., 2010. Detecting trend and seasonal changes in satellite image time series. Remote Sens. Environ. 114, 106–115. https://doi.org/10.1016/j.rse.2009.08.014.
Vicente-Serrano, S.M., Beguería, S., López-Moreno, J.I., 2010. A multiscalar drought index sensitive to global warming: the standardized precipitation evapotranspiration index. J. Clim. 23, 1696–1718. https://doi.org/10.1175/2009JCLI2909.1.
Vicente-Serrano, S.M., Camarero, J.J., Olano, J.M., Martín-Hernández, N., Peña-Gallardo, M., Tomás-Burguera, M., Gazol, A., Azorin-Molina, C., Bhuyan, U., El Kenawy, A., 2016. Diverse relationships between forest growth and the Normalized Difference Vegetation Index at a global scale. Remote Sens. Environ. 187, 14–29. https://doi.org/10.1016/j.rse.2016.10.001.
Vicente-Serrano, S.M., Tomas-Burguera, M., Beguería, S., Reig, F., Latorre, B., Peña-Gallardo, M., Luna, M.Y., Morata, A., González-Hidalgo, J.C., 2017. A high resolution dataset of drought indices for Spain. Data 2, 22. https://doi.org/10.3390/data2030022.
Wang, X., Piao, S., Ciais, P., Li, J., Friedlingstein, P., Koven, C., Chen, A., 2011. Spring temperature change and its implication in the change of vegetation growth in North America from 1982 to 2006. Proc. Natl. Acad. Sci. 108, 1240–1245. https://doi.org/10.1073/pnas.1014425108/-/DCSupplemental.
White, M.A., Thornton, P.E., Running, S.W., 1997. A continental phenology model for monitoring vegetation responses to interannual climatic variability. Glob. Biogeochem. Cycles 11, 217–234. https://doi.org/10.1029/97GB00330.
White, M.A., de Beurs, K.M., Didan, K., Inouye, D.W., Richardson, A.D., Jensen, O.P., O'Keefe, J., Zhang, G., Nemani, R.R., van Leeuwen, W.J.D., Brown, J.F., de Wit, A., Schaepman, M., Lin, X., Dettinger, M., Bailey, A.S., Kimball, J., Schwartz, M.D., Baldocchi, D.D., Lee, J.T., Lauenroth, W.K., 2009. Intercomparison, interpretation, and assessment of spring phenology in North America estimated from remote sensing for 1982-2006. Glob. Chang. Biol. 15, 2335–2359. https://doi.org/10.1111/j.1365-2486.2009.01910.x.
Wilson, E.H., Sader, S.A., 2002. Detection of forest harvest type using multiple dates of Landsat TM imagery. Remote Sens. Environ. 80, 385–396. https://doi.org/10.1016/S0034-4257(01)00318-2.
Wood, S., 2003. Thin plate regression splines. J. R. Stat. Soc. Ser. B (Stat. Methodol.) 65, 95–114. https://doi.org/10.1111/1467-9868.00374.
Wood, S.N., 2017. Generalized Additive Models: An Introduction With R. Chapman and Hall/CRC, Second. ed.
Xulu, S., Peerbhay, K., Gebreslasie, M., Ismail, R., 2018. Drought influence on forest plantations in Zululand, South Africa, using MODIS time series and climate data. Forests 9, 528. https://doi.org/10.3390/f9090528.
Zhang, Y., Peng, C., Li, W., Fang, X., Zhang, T., Zhu, Q., Chen, H., Zhao, P., 2013. Monitoring and estimating drought-induced impacts on forest structure, growth, function, and ecosystem services using remote-sensing data: recent progress and future challenges. Environ. Rev. 21, 103–115. https://doi.org/10.1139/er-2013-0006.
Zhao, W., Zhao, X., Zhou, T., Wu, D., Tang, B., Wei, H., 2017. Climatic factors driving vegetation declines in the 2005 and 2010 Amazon droughts. PLoS One 12, e0175379. https://doi.org/10.1371/journal.pone.0175379.
Zhao, K., Hu, T., Li, Y., 2019a. Rbeast: Bayesian Change-Point Detection and Time Series Decomposition.
Zhao, K., Wulder, M.A., Hu, T., Bright, R., Wu, Q., Qin, H., Li, Y., Toman, E., Mallick, B., Zhang, X., Brown, M., 2019b. Detecting change-point, trend, and seasonality in satellite time series data to track abrupt changes and nonlinear dynamics: A Bayesian ensemble algorithm. Remote Sens. Environ. 232, 111181. https://doi.org/10.1016/j.rse.2019.04.034.
Zuur, A., Ieno, E.N., Walker, N., Saveliev, A.A., Smith, G.M., 2009. Mixed effects models and extensions in ecology with R. Springer, New York.